International Journal of Fluid Power 10 (2009) No. 2 pp. 29-43

POWER LOSS IN THE LUBRICATING GAP BETWEEN CYLINDER BLOCK AND VALVE PLATE OF SWASH PLATE TYPE AXIAL PISTON MACHINES

Monika Ivantysynova[1] and Jonathan Baker[2]

[1]*Purdue University, Department of Agricultural and Biological Engineering, 225 S. University Street, West Lafayette, IN 47907, USA*
[2]*Purdue University, Maha Fluid Power Research Center, 1500 Kepner Dr., Lafayette, IN 47906, USA*
mivantys@purdue.edu, jebaker@purdue.edu

Abstract

The lubricating gaps are the primary source of energy dissipation in piston machines. The paper presents results of a simulation study that investigates the effect that a wave-like micro surface shape variation applied to the valve plate gap surface has on power loss in the cylinder block-valve plate interface. Special attention is given to the relation between gap height, operating parameters, surface design and power loss. The effect of waved surface amplitude and frequency is also studied. Results indicate that power loss in the cylinder block-valve plate interface can be reduced by over 50 % on account of the waved surface compared to the standard cylinder block-valve plate interface design. The effect of the waved surface is most significant at low operating pressures. A special in-house code has been used for this research study. The simulation model covers fluid-structure interaction and micro motion of the cylinder block resulting from oscillating piston forces. Details of the model are explained. The model predicts the pressure and velocity fields generated in the lubricating film and calculates leakage, viscous friction and power loss.

Keywords: lubricating gaps, cylinder block-valve plate, axial piston pump, waved surface, energy dissipation

1 Introduction

This paper concerns the cylinder block-valve plate interface of axial piston machines. The authors present for the first time a fluid-structure interaction model that is used to investigate methods of reducing the power loss generated in this interface. The model used in this paper has been developed by (Wieczorek and Ivantysynova, 2002) and (Huang and Ivantysynova, 2003) and is part of the in-house simulation code CASPAR. CASPAR models the interaction of oscillating external and fluid forces and predicts the time dependent gap heights and fluid film conditions of the three connected sealing and bearing interfaces of the rotating group of swash plate type axial piston machines, shown in Fig. 1. The gap heights are determined in the model by solving for the force balance between external and fluid forces for each time step while considering micro-motion of the moveable parts. The fluid film interaction model used for this study will be explained in the following chapter.

Using the model, an extensive simulation study has been carried out by (Baker, 2008) investigating the power loss in the cylinder block-valve plate interface as a function of operating parameters, machine design, and gap height. The study concludes that, at low operating loads, the cylinder block-valve plate gap alone contributes between 60 % and 70 % to all power losses associated with the lubricating gaps (Baker, 2008).

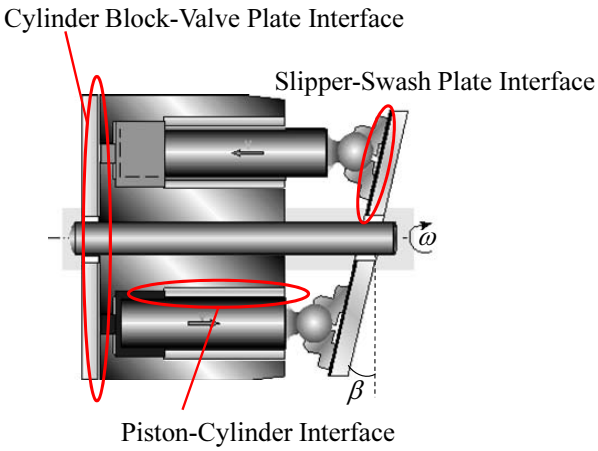

Fig. 1: *Cross section of an axial piston machine of swash plate design illustrating the three lubricating gaps*

This manuscript was received on 26 February 2009 and was accepted after revision for publication on 12 May 2009

The relatively high losses at low pressure and low displacement operating conditions limit the overall machine efficiency at these conditions. In this paper a micro-structured waved surface applied to the valve plate gap surface is presented as a method for reducing these losses.

2 The Simulation Model CASPAR

2.1 Background and Gap Flow

The lubricating gap between the cylinder block and valve plate serves two important functions necessary for proper machine operation. First, the gap serves to seal the individual displacement chambers. Second, the gap provides a combined hydrostatic-hydrodynamic axial sliding bearing that supports the cylinder block.

Full lubrication between the cylinder block and valve plate is maintained only when the resulting fluid force, F_{Fz}, and the moments caused by the fluid force, M_{Fx} and M_{Fy}, generated in the lubricating gap balance the external force, F_{Bz}, and external moments, M_{Bx} and M_{By}, acting on the cylinder block. The model is used to design the cylinder block-valve plate gap in a way that guarantees a sufficient lubricating film throughout a wide range of operating parameters and provides the design engineer with a method for minimizing the power loss due to leakage and viscous friction.

The model considers all time dependent external forces and moments, which are required to be balanced by the hydrodynamic pressure field generated in the fluid film. The force balance is used to determine the gap height, $h_B(r,\varphi)$, at each grid point of the fluid grid for each time step. The model considers the local change of gap height caused by the elastic surface deformation of the cylinder block and the impact that this has on the resulting hydrodynamic pressure field. The fluid film model considers laminar flow, which can be described using the Reynolds Equation derived for a polar coordinate system illustrated in Fig. 2.

The Reynolds Equation in polar coordinates - refer to (Huang and Ivantysynova, 2003) - is given below:

$$\frac{1}{r}\frac{\partial p}{\partial r}h_B^3+\frac{\partial}{\partial r}\left(\frac{\partial p}{\partial r}h_B^3\right)+\frac{1}{r^2}\frac{\partial}{\partial \varphi}\left(\frac{\partial p}{\partial \varphi}h_B^3\right)= 6\mu\left(\omega\frac{\partial h_B}{\partial \varphi}+2\frac{\partial h_B}{\partial t}\right) \tag{1}$$

Equation 1 demonstrates the high degree of dependence of the Reynolds Equation on the gap height, $h_B(r,\varphi)$. The model calculates the gap height between the cylinder block and valve plate in three points, h_{B1}, h_{B2} and h_{B3}, illustrated in Fig. 2. Based on these three points, the gap height for each grid point can be calculated:

$$h_B(r,\varphi)=r\sin\varphi\frac{\sqrt{\frac{1}{3}}}{R_{Ba}}(h_{B2}-h_{B3})+ r\cos\varphi\frac{1}{3R_{Ba}}(2h_{B1}-h_{B2}-h_{B3})+ \frac{1}{3}(h_{B1}-h_{B2}-h_{B3})+\Delta h \tag{2}$$

The vector $\mathbf{h}_B$, representing the three points, h_{B1}, h_{B2} and h_{B3}, is calculated by assuming a force balance between the external and fluid forces. These forces are illustrated in Fig. 3.

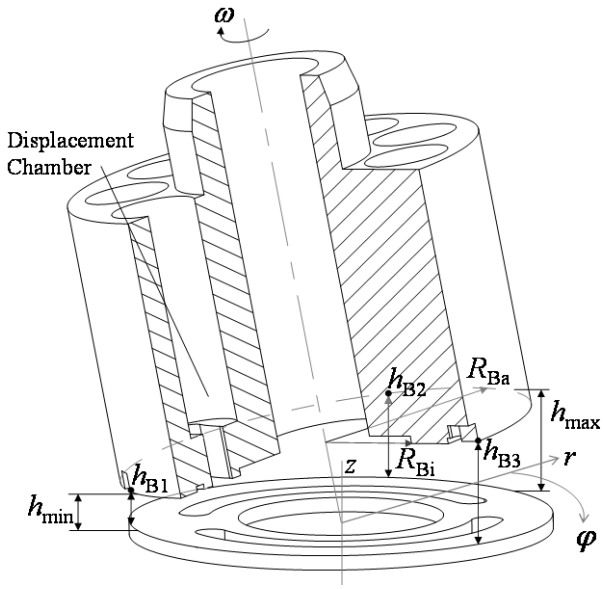

Fig. 2: *Illustration of the lubricating gap between cylinder block and valve plate*

2.2 External Forces

The external forces acting along the *x*, *y*, and *z* axes are calculated as follows:

$$F_{Bx}=\sum_{i=1}^{z}F_{RBxi} \tag{3}$$

$$F_{By}=\sum_{i=1}^{z}F_{RByi} \tag{4}$$

$$F_{Bz}=-F_{FB}+\sum_{i=1}^{z}F_{DBi}+\sum_{i=1}^{z}F_{TBzi} \tag{5}$$

The moments about the *x*, *y* and *z* axes can be calculated using the following equations:

$$M_{Bx}=\sum_{i=1}^{z}y_i F_{DBi}+\sum_{i=1}^{z}y_i F_{TBzi}-\sum_{i=1}^{z}z_i F_{RByi} \tag{6}$$

$$M_{By}=-\sum_{i=1}^{z}x_i F_{DBi}-\sum_{i=1}^{z}x_i F_{TBzi}+\sum_{i=1}^{z}z_i F_{RBxi} \tag{7}$$

$$M_{Bz}=\sum_{i=1}^{z}x_i F_{RByi}+\sum_{i=1}^{z}y_i F_{RBxi}+M_{TBz} \tag{8}$$

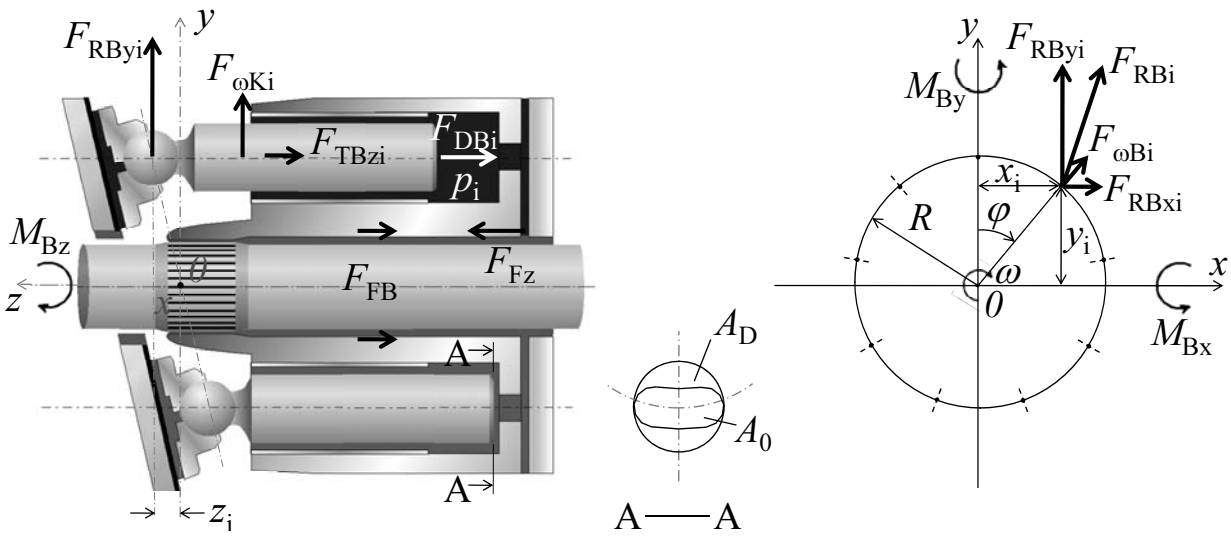

Fig. 3: *Illustration of the external and fluid forces considered by the cylinder block-valve plate model*

The pressure generated in the fluid film between the cylinder block and valve plate must balance the external force F_{Bz} and moments M_{Bx} and M_{By} (Eq. 5 to 7 respectively). The remaining forces (Eq. 3 and Eq. 4) are supported by the shaft bearings. The moment M_{Bz} represents the torque of the pump and is not needed to calculate the gap height. In principle, M_{TBz} represents the torque losses due to viscous friction in the cylinder block-valve plate interface as well as the torque losses due to churning and the torque losses due to the shaft bearings. There is, however, no model to describe either of these later two torque losses. For this reason, in practice, M_{TBz} only describes the torque losses due to viscous friction in the cylinder block-valve plate interface.

The following discussion explains in greater detail the calculations of Eq. 5, Eq. 6 and Eq. 7. In Eq. 5, F_{FB} is the spring force acting on the block (Fig. 3). F_{TBzi} represents the friction force acting on the cylinder block due to friction between the piston and cylinder bore. This force is simply the opposite of the piston friction force, F_{TKi}, calculated by the gap flow simulation for the piston-cylinder gap:

$$F_{TBzi} = -F_{TKi} \tag{9}$$

Note that F_{TBzi} is always acting in the direction of piston movement. The radial piston forces, F_{RBxi} and F_{RByi}, transferred to the cylinder block are calculated by:

$$F_{RBxi} = F_{wKi} \sin\varphi - F_{TGi} \cos\varphi \tag{10}$$

$$F_{RByi} = F_{SKyi} + F_{wKi} \cos\varphi + F_{TGi} \sin\varphi \tag{11}$$

$F_{\omega Ki}$ is the centrifugal force acting on an individual piston, F_{TGi} is the slipper friction force of an individual slipper caused by movement between the slipper and swash plate, and F_{SKyi} is the y component of the the swash plate reaction force for an individual piston-slipper assembly. $F_{\omega Ki}$ and F_{SKyi} are calculated in the gap flow model of the piston-cylinder interface, and F_{TGi} is calculated in the gap flow model of the slipper-swash plate interface.

Finally, F_{DBi} represents the oscillating axial pressure force caused by the instantaneous cylinder pressure, p_i, acting on the displacement chamber area, A_D, illustrated in Fig. 3. This force is calculated for each individual displacement chamber:

$$F_{DBi} = -p_i A_D \tag{12}$$

2.3 Instantaneous Cylinder Pressure

The calculation of instantaneous cylinder pressure, p_i, assumes a compressible fluid and is based on the pressure build up equation:

$$p_i = \frac{K}{V_i}\left(Q_{ri} - Q_{SKi} - Q_{SGi} - Q_{SBi} - \frac{dV_i}{dt} \right) \tag{13}$$

where K is the bulk modulus, V_i is the volume of the displacement chamber, Q_{ri} is the flow into the displacement chamber during suction stroke of the piston and out of the displacement chamber during the discharge stroke, and Q_{SKi} and Q_{SGi} are the leakage flows through an individual piston-cylinder and slipper-swash plate gap respectively. Q_{SBi} is the leakage through the cylinder block-valve plate gap, Q_{SB}, divided by the number of pistons. Q_{SKi}, Q_{SGi} and Q_{SB} are outputs of each respective gap flow calculation.

In pratice, there is no such quantity as individual leakage, Q_{SBi}, for the cylinder block. In order to avoid overestimating the leakage when summing over the number of pistons, Q_{SBi} is taken as the leakage through the gap divided by the number of pistons.

Q_{ri} is calculated by the orifice equation:

$$\begin{aligned} Q_{ri} = {} & \alpha_D A_{rHD} \sqrt{\frac{2|p_i - p_{HP}|}{\rho}} \cdot \\ & \operatorname{sgn}(p_i - p_{HP}) + \alpha_D A_{rND} \cdot \\ & \sqrt{\frac{2|p_i - p_{LP}|}{\rho}} \operatorname{sgn}(p_i - p_{LP}) \end{aligned} \tag{14}$$

where α_D is an orifice coefficient, A_{rHD} and A_{rND} are the area openings of the high pressure and low pressure ports respectively, p_i is the instantaneous cylinder pres-

sure, p_{HP} and p_{LP} are the high and low pressure operating conditions set by the user and ρ is the fluid density.

An example of the instantaneous cylinder pressure for an individual displacement chamber over one shaft revolution is shown below in Fig. 4 as a function of shaft rotation angle φ. The displacement chamber pressure is high for the first 180° of rotation, indicating the piston to be in discharge stroke. For the later 180° of rotation, the displacement chamber pressure is low, indicating that the piston is undergoing suction stroke. Flow ripple and effective flow rate at the pump outlet are also calculated in the pressure simulation.

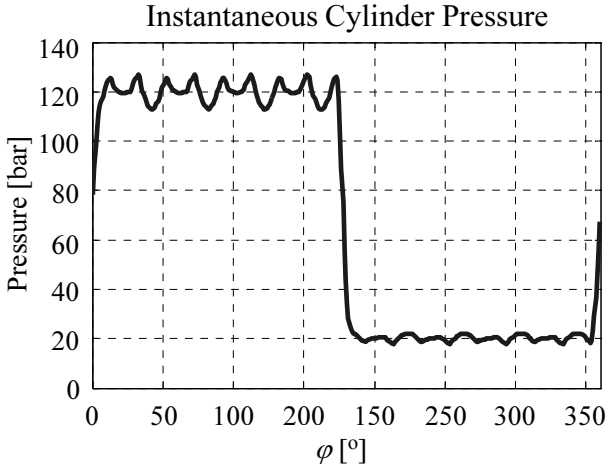

Fig. 4: *Example of the instantaneous cylinder pressure over one shaft revolution calculated by the pressure simulation*

2.4 Fluid Forces

The fluid force, F_{Fz}, or load capacity of the cylinder block-valve plate gap can be calculated from the pressure distribution (i.e. the pressure at each grid point), $p_{i,j}$, which is the solution to the Reynolds Equation (Eq. 1):

$$F_{Fz} = \sum_{i=0}^{N}\sum_{j=0}^{M} p_{i,j} r_{i,j} \Delta r \Delta \varphi \tag{15}$$

The moments about the x and y axes, M_{Fx} and M_{Fy} respectively, caused by the fluid force, F_{Fz}, can be calculated:

$$M_{Fx} = \sum_{i=0}^{N}\sum_{j=0}^{M} F_{Fzi,j} y_{i,j} \tag{16}$$

$$M_{Fy} = \sum_{i=0}^{N}\sum_{j=0}^{M} -F_{Fzi,j} x_{i,j} \tag{17}$$

2.5 Force Balance

Full lubrication in the cylinder block-valve plate gap is ensured by considering a balance of forces between the fluid forces and external forces, derived in the preceding sections. The force balance is achieved by solving the motion equation, shown below:

$$\begin{pmatrix} F_{Fz}\left(\dot{\boldsymbol{h}}_B, \boldsymbol{h}_B, t\right) + F_{Bz}(t) \\ M_{Fx}\left(\dot{\boldsymbol{h}}_B, \boldsymbol{h}_B, t\right) + M_{Bx}(t) \\ M_{Fy}\left(\dot{\boldsymbol{h}}_B, \boldsymbol{h}_B, t\right) + M_{By}(t) \end{pmatrix} = 0 \tag{18}$$

2.6 Fluid-Structure Interaction

As can be seen from Eq. 1, the gap flow model is highly sensitive to changes in the gap height, $h_B(r,\varphi)$. The final component to the cylinder block-valve plate gap model is a description of the local change in gap height, Δh, on account of elastic surface deformation caused by the pressure field in the gap. This effect was first described by (Huang and Ivantysynova, 2003) for the cylinder block-valve plate gap. In the current model, only surface deformation on the cylinder block gap surface is considered significant. In principle, the valve plate would deform as well. Deformation, however, is proportional to the part thickness and the valve plate is rather thin. Deformation on the valve plate is therefore neglected.

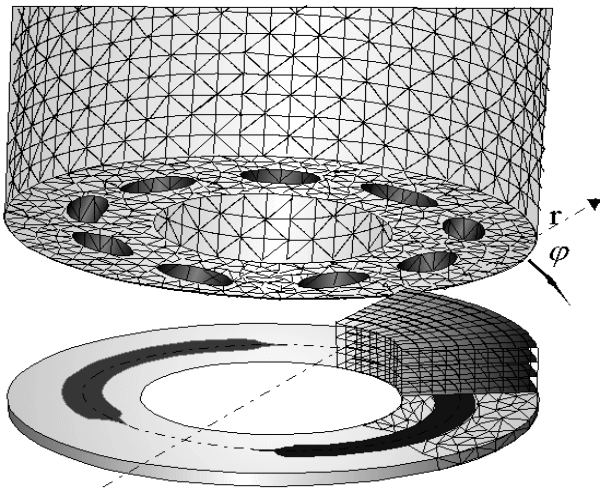

Fig. 5: *Illustration of the fluid and structural mesh for the cylinder block-valve plate gap*

The described, and in this work considered, surface deformation of the cylinder block represents a fluid structure interaction problem and needs to be modeled and solved as such. The method used in CASPAR is to match the fluid grid with the structure grid and then apply pressure from each fluid grid element to each corresponding solid grid element. Figure 5 illustrates an example of the fluid and structural mesh.

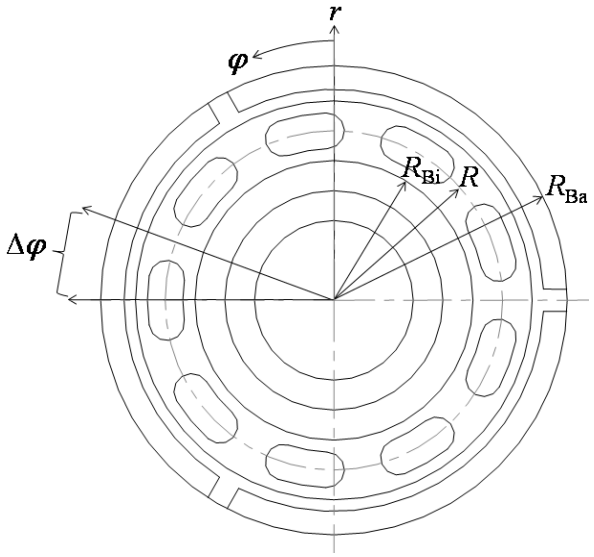

Fig. 6: *Illustration of the section of the cylinder block, Δφ; z points into the page*

Calculating deformation involves finite element theory. The finite element analysis is done outside of the model using the commercial software tool ANSYS and a 100 bar reference pressure. Deformation is calculated on the entire gap surface due to pressure applied to a small area surrounding a single grid point on the gap surface. The output of this calculation is one influence matrix, $\mathbf{u}_{\mathrm{ref}}$, a function of radial and circumferential grid position. Due to axes of symmetry, it is unnecessary to calculate an influence matrix for each grid point of the gap surface. Influence matrices are calculated within a representative region of the cylinder block gap surface, $\Delta\varphi$, illustrated in Fig. 6.

The cylinder block surface will also deform due to pressure in the displacement chamber. An additional influence matrix, $\mathbf{u}_{\mathrm{bDC}}$, is therefore calculated based on a 100 bar reference pressure applied to area A_{D} shown in Fig. 3.

The total plane of deformation due to the pressure distribution p_{final} is calculated using a linear relationship shown below:

$$\mathbf{\Delta h} = \sum_{i=0}^{N}\sum_{j=0}^{M}\frac{p_{\mathrm{final}_{i,j}}}{100\ \mathrm{bar}}\cdot\left[\mathbf{u}_{\mathrm{ref}}\right]_{i,j} + \sum_{i=0}^{k_{\mathrm{no}}}\frac{p_{\mathrm{i}}}{100\ \mathrm{bar}}\cdot\left[\mathbf{u}_{\mathrm{bDC}}\right] \tag{19}$$

where in the first addend of Eq. 19, i and j refer to the radial and circumferntial position and in the second addend of Eq. 19, i refers to the displacment chamber index. The total deformation applied to the gap due to the pressure in the fluid film and pressure in the displacement chamber is in a range of tenths of microns to approximately one micron.

Deformation is not solely driven by pressure. It is understood that high temperature gradients existing in axial piston pumps likely cause thermoelastic deformation. Though preliminary investigation into this effect is underway (Pelosi and Ivantysynova, 2009) thermoelastic deformation is not considered here.

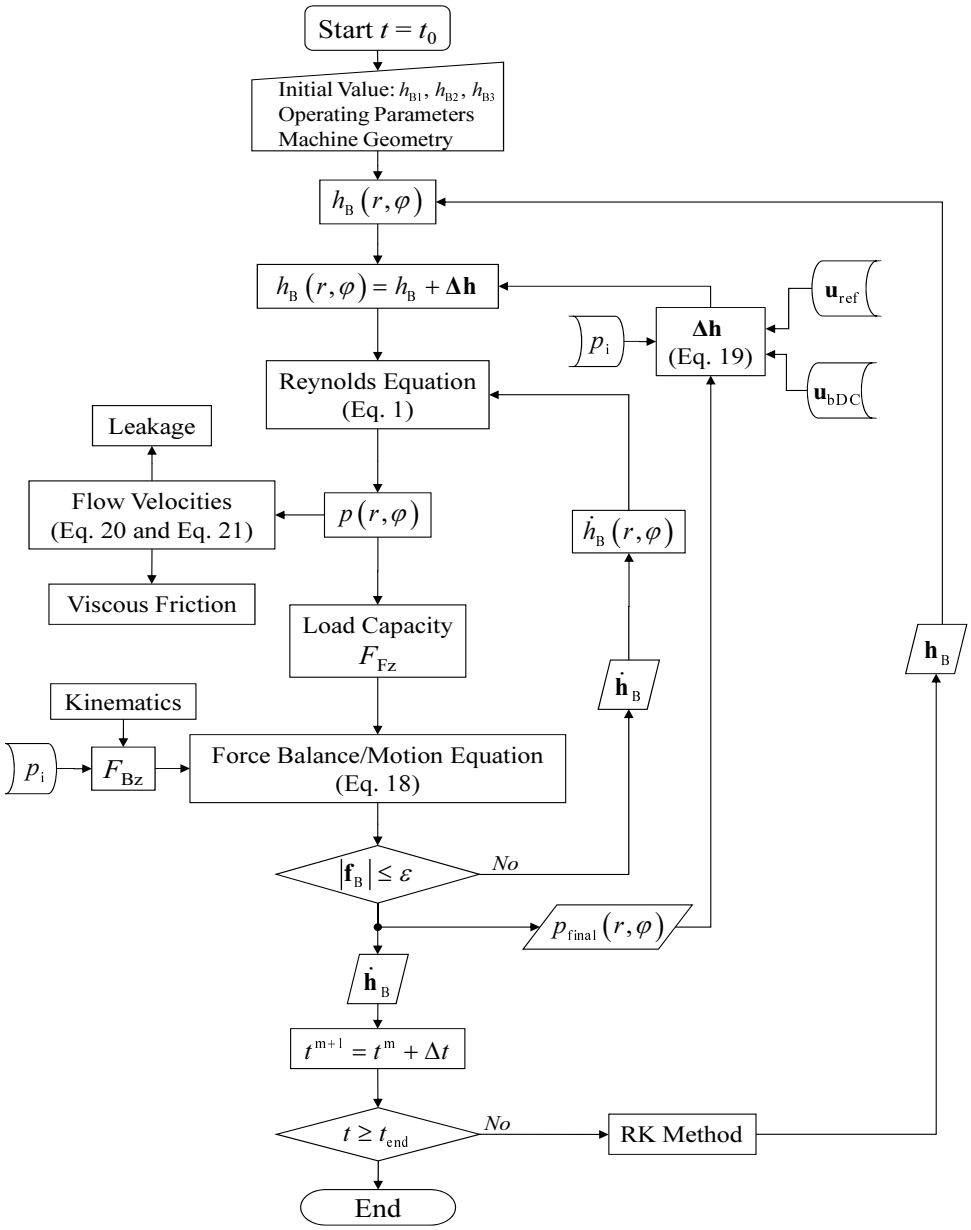

Fig. 7: *Program structure for the cylinder block valve plate model implemented in CASPAR*

2.7 Model Structure

The cylinder block-valve plate interface model structure is illustrated in Fig. 7. The gap height serves as an input to the Reynolds Equation, the output of which is the pressure distribution in the gap. The pressure distribution is used to calculate the flow velocity fields and consequentially the losses due to leakage and viscous friction. The pressure distribution is also used to calculate the load capacity of the gap (i.e. fluid forces). These must be balanced with external forces, which are calculated from the pump kinematics and the pressure simulation and have been derived in the preceding sections. Using a Newton iteration scheme, the model iterates on the shifting velocity, $h_B(r,\varphi)$, until a force balance is achieved. After achieving a force balance, the model proceeds to the next time step. The shifting velocity that achieves the force balance is integrated and a new value of $h_B(r,\varphi)$ is obtained. Before inputting the new $h_B(r,\varphi)$ back into the Reynolds Equation, deformation on the cylinder block surface due to pressure in the gap is considered. The pressure distribution from the final Newton iteration, $p_{final}(r,\varphi)$, as well as the pressure in each displacement chamber, p_i, is used to calculate deformation on the entire gap surface, $\Delta\mathbf{h}$. The deformation is added to the gap surface, thereby achieving the gap height that is input back into the Reynolds Equation. The process repeats until the time, t, reaches the user defined value of t_{end} or the simulation is terminated by the user.

A simulation is generally stopped when the block position has stabilized, i.e. the j^{th} revolution would look similar to the $j^{th}+1^{st}$ revolution. An example of a stabilized block position over one shaft revolution is illustrated in Fig. 8. The three points, h_{B1}, h_{B2}, and h_{B3} are illustrated in Fig. 2. Though the position is said to be stable, h_{B1}, h_{B2}, and h_{B3} all oscillate about a mean value. The oscillating axial forces caused by the finite number of pistons cause these oscillations.

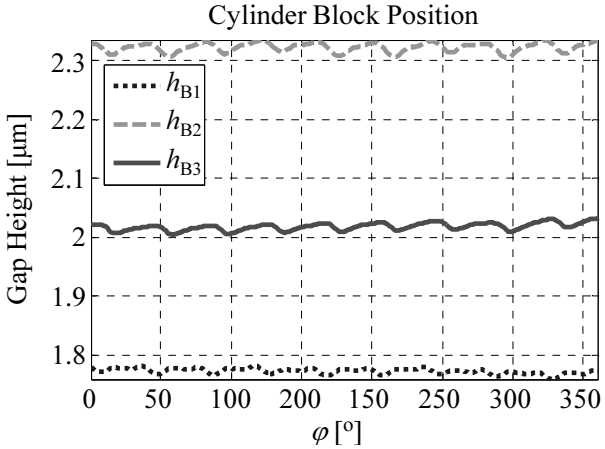

Fig. 8: *Two dimensional illustration of the cylinder block position with respect to the valve plate over one shaft revolution (refer to Fig. 2 for an illustration of h_{B1}, h_{B2}, and h_{B3})*

2.8 Power Losses

Aside from forces, the pressure distribution also makes possible a prediction of the radial and circumferential velocity fields, v_r and v_φ, in the gap between cylinder block and valve plate:

$$v_r = \frac{1}{2\mu}\frac{\partial p}{\partial r}\left(z^2 - h_B z\right) \tag{20}$$

$$v_j = \frac{1}{2\mu}\frac{\partial p}{r\partial \varphi}\left(z^2 - h_B z\right) + \omega r\frac{z}{h} \tag{21}$$

where μ is the dynamic oil viscosity. It should be noted that whereas only Poiseuille flow is considered for the radial velocity field (Eq. 20), both Poiseuille and Couette flow are considered for the circumferential component of velocity (Eq. 21).

The velocity fields are used to calculate the radial and circumferential friction force components, F_{TBr} and $F_{TB\varphi}$, as well as the torque losses due to viscous friction, M_{TBz} (recall from the discussion in section 2.2 that M_{TBz} would also in principle include torque losses due to churning and shaft bearings, but owing to the absence of models for these losses, they are not included here):

$$F_{TBr} = \int_A \tau_r dA = \int_0^{2\pi}\int_{R_{Bi}}^{R_{Ba}} \mu\frac{\partial v_r}{\partial z} r dr d\varphi \tag{22}$$

$$F_{TBj} = \int_A \tau_j dA = \int_0^{2\pi}\int_{R_{Bi}}^{R_{Ba}} \mu\frac{\partial v_j}{\partial z} r dr d\varphi \tag{23}$$

$$M_{TBz} = \int_A r\tau dA = \int_0^{2\pi}\int_{R_{Bi}}^{R_{Ba}} \mu\frac{\partial v_j}{\partial z} r^2 dr d\varphi \tag{24}$$

where τ is the shear stress. The leakage through the cylinder block valve plate, Q_{SB}, can be calculated from the velocity fields as well. There are two components of leakage; leakage flowing out of the gap at $r = R_{Ba}$ (in the positive radial direction), Q_{SBe1}, and leakage flowing out of the gap at $r = R_{Bi}$ (in the negative radial direction), Q_{SBe2}.

$$Q_{SB} = Q_{SBe1} + Q_{SBe2} = \int_0^{2\pi}\int_0^h v_r r dz\, d\varphi\Big|_{r=R_{Ba}} + \int_0^{2\pi}\int_0^h -v_r r dz\, d\varphi\Big|_{r=R_{Bi}} \tag{25}$$

In order to evaluate the performance of various pump designs or, in the case of this paper, various waved surfaces, power loss due to viscous friction and leakage, P_f and P_Q respectively, are calculated:

$$P_f = 2\pi n M_{TBz} \quad \text{and} \quad P_Q = \left(p_i - p_{case}\right) Q_{SB} \tag{26}$$

Total power loss in the cylinder block valve plate gap is calculated by summing the two components of losses displayed in Eq. 26:

$$P_{tot} = P_f + P_Q \tag{27}$$

2.9 Dynamic Viscosity

The change of dynamic fluid viscosity with temperature is an important effect. The model in this study assumes a constant temperature on the surfaces of the cylinder block and valve plate. The temperature at each grid point within the fluid mesh used to calculate the dynamic viscosity is interpolated between these two surface temperatures. It is well understood, however, that surface temperature distributions of the cylinder block and valve plate are not constant. A recent study

(Jouini and Ivantysynova, 2008) implemented a thermal model for the cylinder block-valve plate interface that considers the change in dynamic viscosity due to the heat generated in the gap. The surface temperature distribution of the cylinder block and valve plate is not assumed to be constant and is determined using a heat transfer model developed for the rotating group. The surface temperatures are used as boundary conditions for the energy equation, the solution of which is the total energy dissipated in the gap. The solution to the energy equation additionally allows the model to consider the fluid temperature in each grid point of the fluid film mesh and therefore the change in the dynamic viscosity with temperature and pressure. The thermal model, however, has not been used due to computational time constraints.

3 The Micro-Structured Waved Surface

3.1 Cylinder Block Sliding Surfaces

It is commonly held that the sliding surfaces of the cylinder block and valve plate (Fig. 9) must be ideally smooth. In this paper, the influence of a waved surface shape of the sealing lands of the cylinder block-valve plate interface on the performance and power loss of the cylinder block valve plate interface of axial piston machines is studied. It is obvious from the governing equation (Eq. 1) describing the hydrodynamic pressure built up in the fluid film that any local change of fluid film thickness contributes to additional hydrodynamic pressure generation. The presented research study investigates whether this effect can be used to reduce the power loss/energy dissipation in this important interface of axial piston machines. Therefore the impact of a sinusoidal waved surface has been investigated. The sinusoidal waved surface can be described with two parameters: the amplitude and frequency of oscillation. The waved surface is illustrated in Fig. 10 for a typical cylindrical cross-section of the valve plate sliding surface.

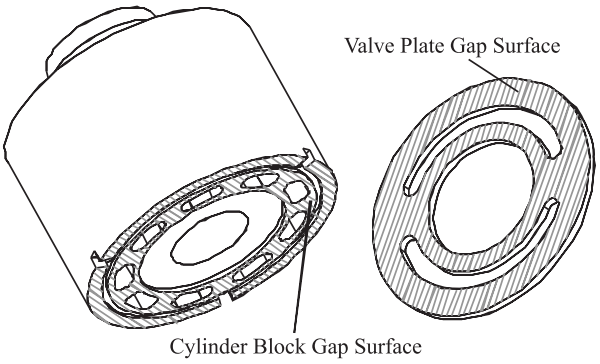

Fig. 9: *Sliding surfaces of the cylinder block-valve plate interface*

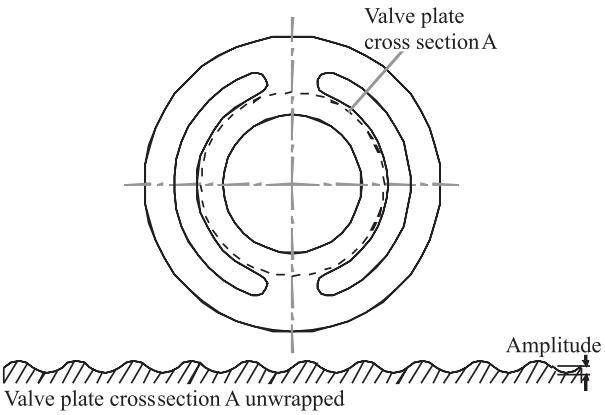

Fig. 10: *Illustration of the waved surface for a typical unwrapped cylindrical cross-section of the valve plate*

3.2 Implementing the Waved Structure in CASPAR

To consider the effect of the waved surface in the model, the gap height (Eq. 2) is modified by adding the appropriate amount to each point of the gap surface. Calculating this amount is achieved in the following way. A sinusoidal wave pattern consisting of any number of oscillations can be fit to a length, C, using the following expression:

$$A\sin\left(\frac{2\pi xf}{C}\right) \tag{28}$$

The variable, x, is descritized by calculating the circumferential spacing between each grid point at each radial position:

$$dC = \frac{C}{M} \tag{29}$$

where C is the circumference of the gap surface at a given radial position and M is the number of grid points in the circumference. The variable, x, at a given radial position is given by:

$$x = jdC \tag{30}$$

where j is the circumferential position index. Substituting Eq. 29 and Eq. 30 into Eq. 28 results in an expression for calculating the waved surface of amplitude A and frequency of oscillation f:

$$A\sin\left(\frac{2\pi jf}{M}\right) \tag{31}$$

The expression in Eq. 31 is calculated for all points r and φ of the cylinder block gap surface and added to the gap height (Eq. 2) at all points r and φ.

3.3 Parameters and Operating Conditions

Eight waved surface combinations, shown in Table 1, are compared to a standard cylinder block-valve plate interface design which considers ideally smooth and flat sliding surfaces. The designs in Table 1, along with the standard design, are simulated at eight operating conditions presented in Table 2.

Table 1: Waved surface parameter combinations

Waved Surface	Frequency [rev^{-1}]	Amplitude [μm]
DM.7	10	+/- 2
DM.8	10	+/- 1
DM.9	15	+/- 1
DM.11	20	+/- 1
DM.12	5	+/- 2
DM.13	15	+/- 0.5
DM.14	15	+/- 2
DM.15	30	+/- 1

Table 2: Operating conditions matrix used to study the waved surface

Sim. No.	Δp [bar]	n [RPM]	p_{HP} [bar]	p_{LP} [bar]	p_{case} [bar]
1	99.0	1000.3	119.8	20.8	1.2
2	298.1	1002.3	319.5	21.5	1.3
3	101.0	3001.6	120.9	19.9	1.4
4	299.7	3001.8	319.4	19.7	1.5
5	99.6	999.8	120.6	21.0	1.3
6	299.5	1000.8	320.5	21.0	1.5
7	101.0	3002.0	121.7	20.8	1.4
8	295.6	3001.3	316.3	20.7	1.5

Sim. No.	T_{HP} [°C]	T_{LP} [°C]	T_{CASE} [°C]	β [%]
1	48.0	47	64.0	100
2	56.0	54	66.9	100
3	52.5	50	90.0	100
4	54.2	48	93.6	100
5	54.5	51	62.3	17.6
6	70.0	55	73.0	17.6
7	53.2	51	91.8	17.6
8	60.9	52	91.4	17.6

The following simulation results through section 3.8 are all for a particular displacement unit geometry, referred to as unit A.

3.4 Gap Heights and Pressure Fields

The gap height and pressure distribution for the cylinder block-valve plate gap simulated at simulation number 1 (Table 2) for one angular position of the cylinder block is illustrated in Fig. 11. The images (a) and (c) are from a standard design. The images (b) and (d) are from the DM.9 waved surface.

Three Dimensional Gap Height and Pressure Fields of the Cylinder Block-Valve Plate Gap

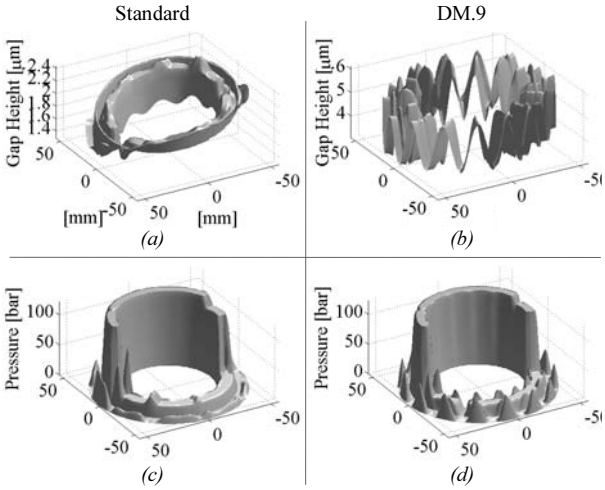

Fig. 11: *Block position and pressure distributions for a standard design (a and c) and DM.9 waved surface (b and d) at φ = 135° at simulation number 1, Table 2*

For each trough in the waved surface shown in Fig. 11b, there is a corresponding peak in the DM.9 pressure field (Fig. 11d). The waved surface, then, induces a micro-hydrodynamic effect that creates an additional load carrying capability of the cylinder block-valve plate gap.

3.5 Average Gap Heights and Power Losses

To futher illustrate the effect of the waved surface, the average maximum and minimum gap height and average power loss data for the standard design, DM.7, DM.8 and DM.9 (Table 1) at simulation numbers 1 and 2 (Table 2) are presented below. The plots of the power loss illustrate the average total power loss as well as power loss due to viscous friction, P_f (P_friction) and power loss due to leakage, P_Q (P_leakage). Average maximum and minimum gap height is calculated using the method described in (Baker, 2008).

The effect of the waved surface at low operating pressure, low speed and full displacement is illustrated in Fig. 12. The gap heights of the waved surface designs are higher than the gap height of the standard design. This is accompanied by a decrease in losses due to viscous friction and an increase in leakage. Since the operating pressure is low, however, the leakage flow rate is minimal and the power loss due to leakage is insignificant. The increase in gap height, therefore, contributes to an overall significant decrease in total power loss at this operating condition; approximately 57 % for the DM.9 waved surface. Similar behaviour is observed for other low pressure operating conditions illustrated in Fig. 14.

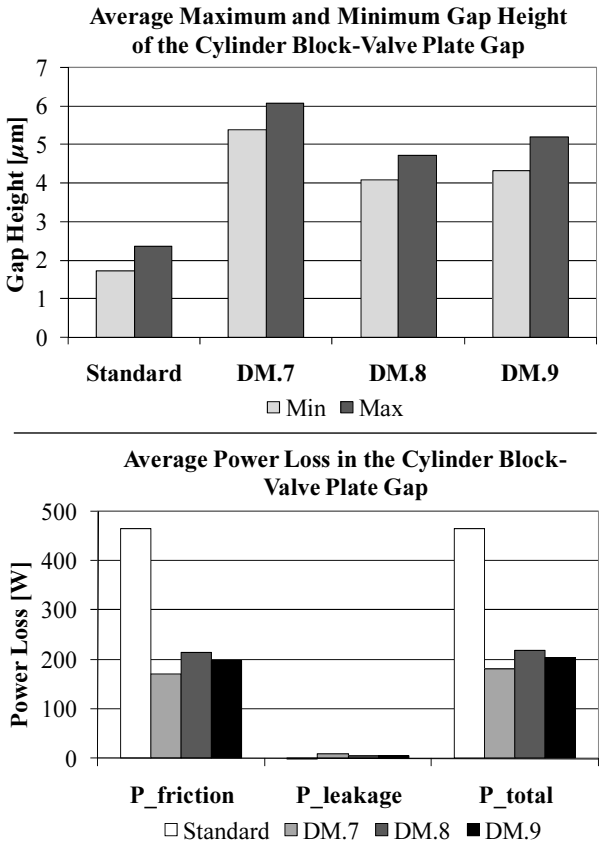

Fig. 12: *Average maximum and minimum gap height and average power loss: simulation number 1, Table 2*

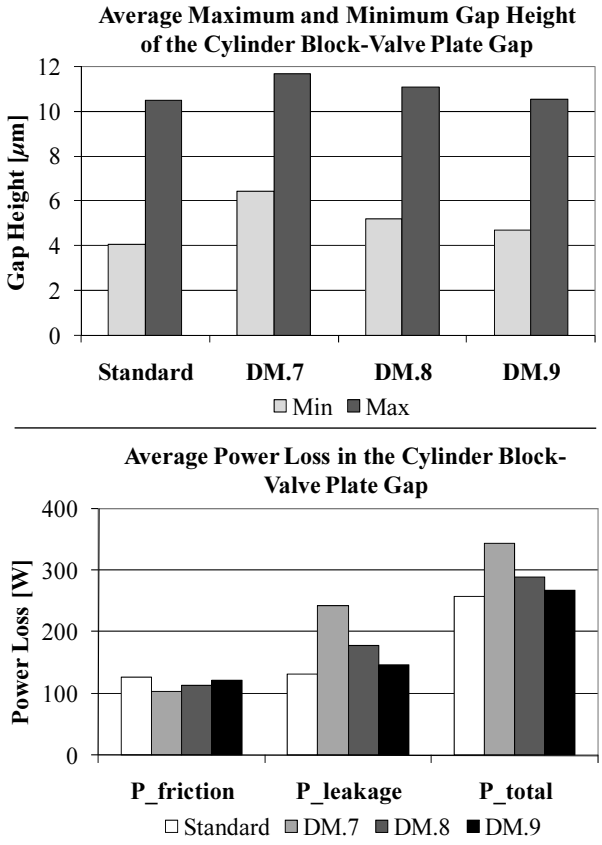

Fig. 13: *Average maximum and minimum gap height and average power loss: simulation number 2, Table 2*

The effect of the waved surface at high operating pressure, low speed and full displacement is illustrated in Fig. 13. Like the case of low pressure, at this higher operating pressure the gap heights of the waved surface designs are higher than the gap height of the standard design. The increase in gap height leads to a corresponding decrease in power loss due to viscous friction, but the decrease is not as large as the decrease observed for low operating pressures. Additionally, unlike the case of low operating pressure, the power loss due to leakage is not insignificant. The increase in gap height leads to an increase in power loss due to leakage that is greater than the decrease in power loss due to viscous friction. Total power loss therefore increases with respect to the standard design, but by less than 1 kW. Similar behaviour is observed for other high pressure operating conditions illustrated in Fig. 14.

The average maximum and minimum gap heights, as well as the average total power losses for the standard design, and the DM.7, DM.8 and DM.9 waved surfaces for all operating condition listed in Table 2 are summarized in Fig. 14.

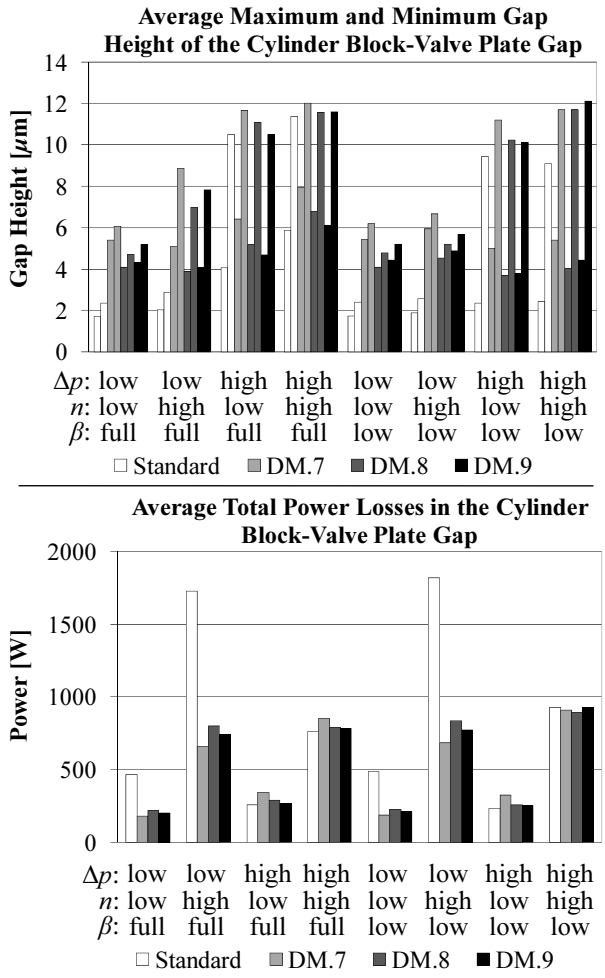

Fig. 14: *Average maximum and minimum gap heights and average total power loss: all operating conditions*

Figure 14 illustrates that significant reductions in power loss can be achieved with the waved surface at low pressure operating conditions, irrespective of operating speed or unit displacement. In general, it is at low pressure operating conditions, and specifically at low pressure and low displacement operating conditions, that pumps experience relatively high power losses. Reducing the losses at these operating conditions in the

cylinder block-valve plate interface brings researchers one step closer to achieving more efficient machines throughout a full range of operating conditions.

Figure 14 also demonstrates that the effect of the waved surface at low pressures is more significant than the effect of the waved surface at high pressures. For example, the DM.9 waved surface achieves an approximately 57 % reduction in power loss at all low operating pressures. At higher operating pressure, the greatest increase in power loss is approximately 9 % due to the DM.9 waved surface.

3.6 The Effect of Amplitude

The effect of wave amplitude can be observed by comparing the standard design with DM.9, DM.13 and DM.14. The standard design can be thought of as a waved surface with zero amplitude. In Fig. 15 below, the data series are arranged in order of increasing amplitude; from left to right zero (standard), +/- 0.5 μm (DM.13), +/- 1 μm (DM.9) and +/- 2 μm (DM.14). The amplitude is held constant at 15 oscillations.

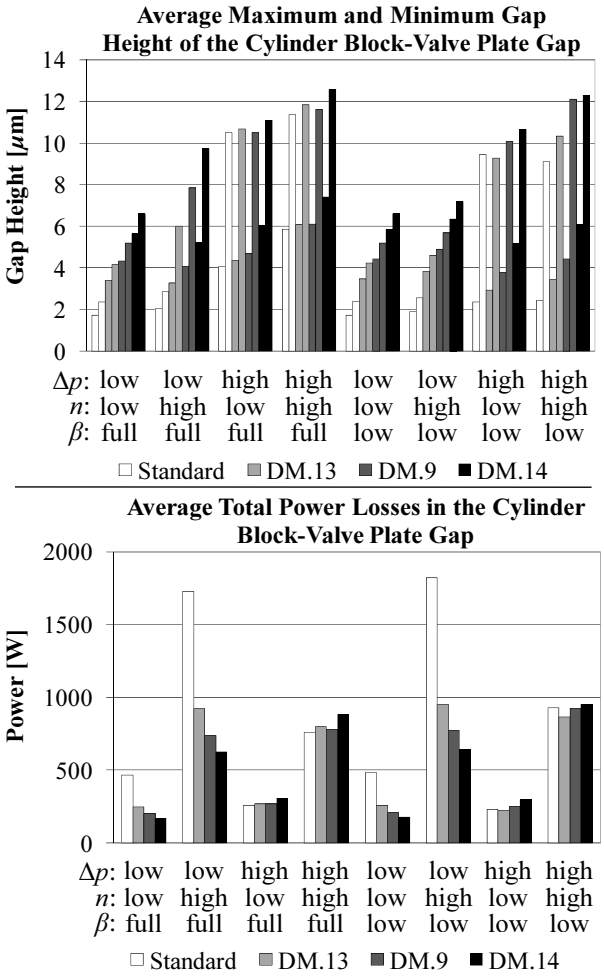

Fig. 15: *Average maximum and minimum gap heights and average total power loss: the effect of amplitude at a constant frequency (15)*

Figure 15 illustrates the average maximum and minimum gap height as well as the average total power loss for the standard design, DM.9, DM.13 and DM.14 at the operating conditions listed in Table 2. The gap height (and therefore load capacity) increases with increasing amplitude. This is in accord with the conclusions of authors who have studied waviness in the past (Hargreaves, 1991; Rasheed, 1998; Ruddy, Dowson and Taylor, 1982[1]). Regarding power loss, at low operating pressure, as amplitude increases, power loss decreases. At higher operating pressures, the opposite is true; as amplitude increases, power loss increases.

3.7 The Effect of Frequency

The effect of wave frequency can be observed by comparing the standard design to DM.8, DM.9, DM.11 and DM.15. The standard design can be thought of as a waved surface with zero frequency. In Fig. 16 below, the data series are arranged in order of increasing frequency; from left to right zero (standard), 10 oscillations (DM.8), 15 oscillations (DM.9), 20 oscillations (DM.11) and 30 oscillations (DM.15). The amplitude is held constant at 1 μm.

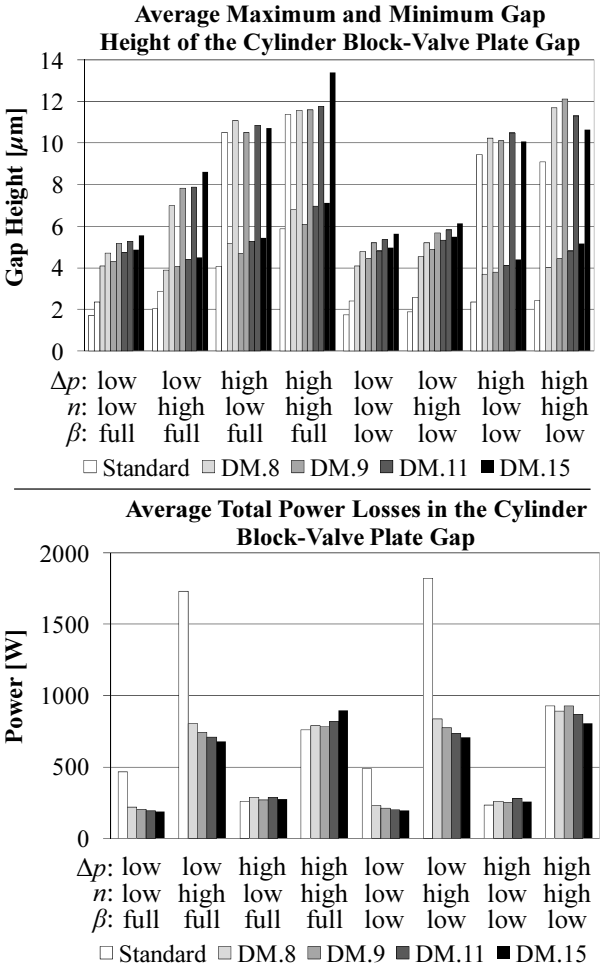

Fig. 16: *Average maximum and minimum gap heights and average total power loss: the effect of frequency at a constant 1 μm amplitude*

Figure 16 illustrates the average maximum and minimum gap height as well as the average total power loss for the standard design, DM.8, DM.9, DM.11 and DM.15 at the operating conditions listed in Table 2. The gap height tends to increases with increasing fre-

[1] This last group of researchers notes, however, that after certain amplitude, gap height begins to decrease.

quency, though not as consistently as was the case with increasing amplitude. Other research in waviness demonstrates that frequency has an effect on load capacity as well (Lebeck, Teale and Pierce; 1978; Rasheed, 1998). Regarding power loss, at low operating pressure, as frequency increases, power loss decreases. At higher pressures, the effect of increasing frequency does not appear to follow a consistent pattern.

3.8 The DM.9 Waved Surface in Motoring Mode

Displacement units often operate in motoring mode. The average maximum and minimum gap height and average total power loss respectively for the standard surface and DM.9 waved surface in both pumping and motoring mode for the operating conditions listed in Table 2 are shown in Fig. 17. As Fig. 17 makes clear, the effect of the DM.9 waved surface in motoring mode is similar to the effect of the DM.9 waved surface in pumping mode.

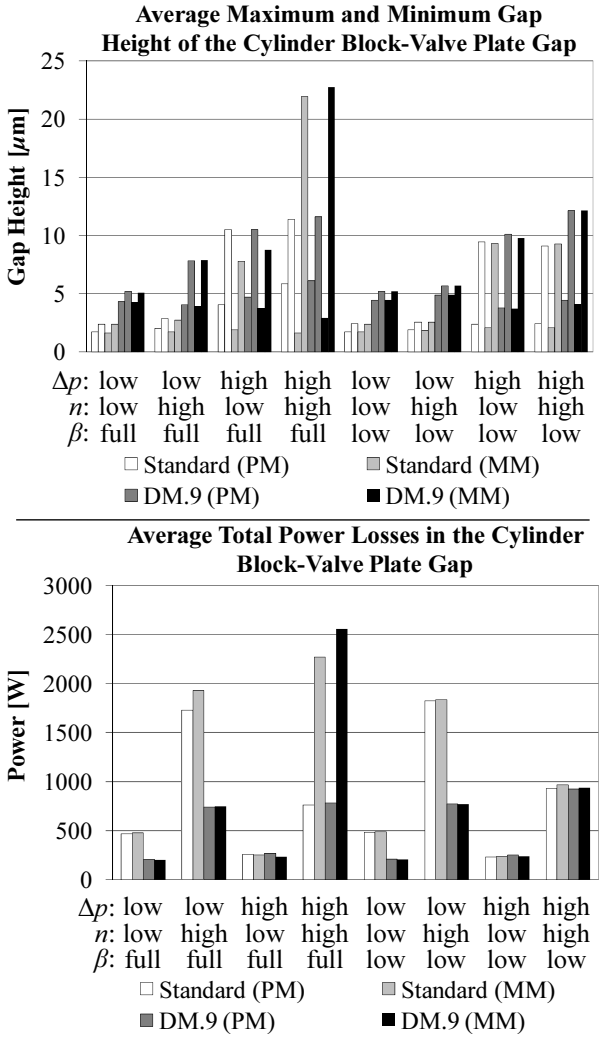

Fig. 17: *Average maximum and minimum gap heights and average total power loss for pumping and motoring mode considering the standard design and DM.9*

3.9 The DM.9 Waved Surface Applied to Alternate Displacement Units

The overall aim of the research is to develop design principles applicable to all displacement machines. Since a high degree of variability exists among current displacement unit designs, the effect of DM.9 applied to two other pump geometries has been investigated. Results from one of these alternate pump geometries, referred to as unit B, is presented below.

The overall effect of the DM.9 waved surface applied to unit B is displayed in Fig. 18, which shows the average maximum and minimum gap heights and the average total power losses for all operating conditions listed in Table 2. Unlike unit A, which only experienced power loss reductions due to the waved surface at low operating pressures, here power loss reductions are achieved at each operating condition. At low operating pressures, reductions are between 52 % and 56 % and at higher operating pressures, reductions are between 15 % and 24 %.

Recall that reductions in power loss were not achieved for unit A at higher operating pressures. The reason that reductions are achieved for unit B at higher operating pressures is because the gap heights of the standard design, shown in Fig. 18, are relatively low (refer to the gap heights of unit A in Fig. 14). For this reason, leakage is also relatively low and unit B can therefore afford an increase in gap height without significantly increasing power loss due to leakage. This is illustrated in Fig. 19.

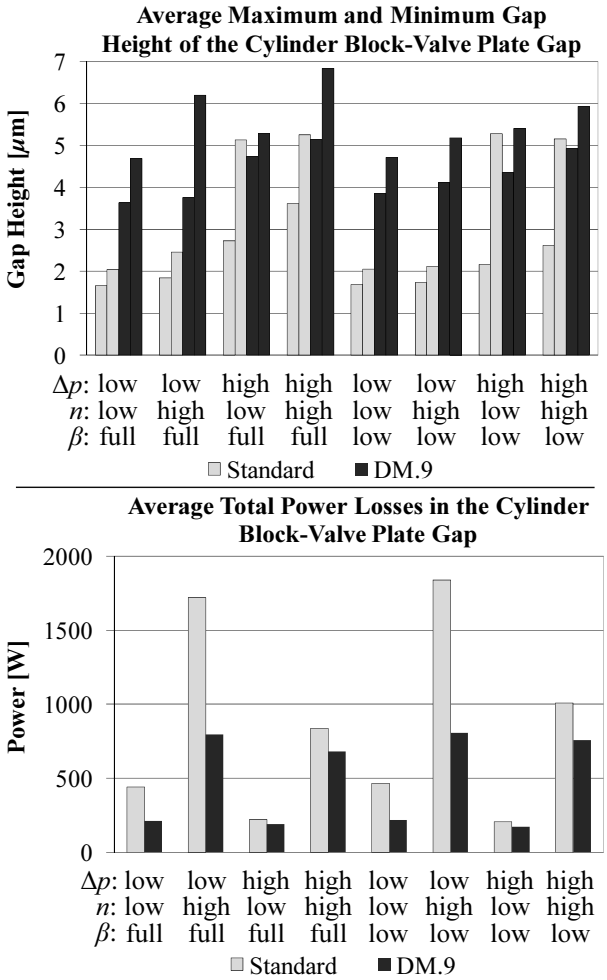

Fig. 18: *Average maximum and minimum gap heights and average total power loss for unit B: Standard and DM.9*

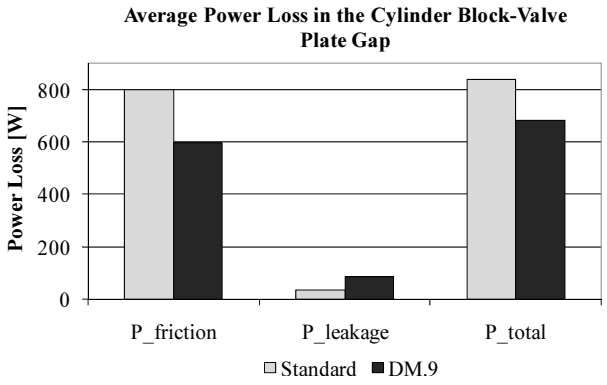

Fig. 19: *Average power loss for unit B at simulation number 4, Table 2, for the standard design and DM.9 waved surface*

4 Conclusion

A model for predicting the gap height and power losses for the cylinder block-valve plate gap has been explained. The model predicts the dynamic gap height between the cylinder block and valve plate by modeling a balance of external and fluid forces as well as micro-motion of the moveable parts. The fluid forces are calculated from a numerical solution to the Reynolds Equation. The model also incorporates a fluid-structure interaction model to describe the local change in gap height due to elastic surface deformation. Currently, research is underway to develop a new model that incorporates the fluid-structure interaction within the calculation loop. The new model is also projected to have faster run times.

The model described is used to investigate the effect that a micro-structured wave surface has on the power loss in the cylinder block-valve plate gap. For both pumping and motoring modes, as well as for various machine geometries and designs, the waved surface is shown to significantly reduce power losses at lower operating pressures at both high and low speed and full and low displacement. Piston machines suffer from relatively high losses at low operating loads (i.e. low pressure and low displacement). The significant reduction of these losses due to the waved surface will help to flatten the efficiency curve by raising the efficiency at low operating loads and maintaining efficiency at high operating loads.

At higher operating pressures, the effect of the waved surface appears to depend on machine design. For unit A, the waved surface increased power loss at higher operating pressures. For unit B, however, the waved surface had the effect of reducing losses regardless of operating pressures, although more significant reductions are achieved at lower operating pressures. The exciting results obtained from applying the waved surface to unit B have motivated the development of a prototype. Efficiency measurements of unit B operating with both the standard valve plate and prototype valve plate demonstrated an increase in total pump efficiency of 2 % to nearly 10 % (Baker and Ivantysynova, 2009).

There are several areas for future work. Continued investigation into the effect of frequency at amplitudes other than 1 μm is one area for further research. It is also of interest to explore, as other authors have done (Yu and Sadeghi, 2001; Vaidya and Sadeghi, 2008), alternatives to a sinusoidal structure. Finally, there are plans to extend this work to the slipper swash-plate interface, owing to the similarities between the cylinder block-valve plate and slipper-swash plate interfaces.

Nomenclature

A	Amplitude of waved surface	[µm]
A_0	Kidney opening area	[m^2]
A_D	Displacement chamber surface area	[m^2]
A_{rHD}	High pressure area opening	[m^2]
A_{rND}	Low pressure area opening	[m^2]
C	Circumference of the cylinder block at a given radial position	[mm]
F_{Bx}, F_{By}, F_{Bz}	External forces on the cylinder block acting along the x and y and z axes	[N]
F_{DBi}	Axial pressure force acting on the cylinder block due to displacement chamber pressure	[N]
F_{FB}	Axial spring force acting on the cylinder block	[N]
F_{Fz}	Fluid force in the cylinder block-valve plate gap (i.e. load capacity)	[N]
F_{RBy}	Radial piston force transferred to the cylinder block acting along the y axis	[N]
F_{Rbxi}, F_{RByi}	Radial piston force from an individual piston acting along the x and y axes	[N]
F_{SKyi}	Swash plate reaction force acting along the y axis	[N]
F_{TBr}	Radial friction force due to viscous friction in the cylinder block-valve plate gap	[N]
$F_{TB\varphi}$	Circumferential friction force due to viscous friction in the cylinder block-valve plate gap	[N]
F_{TBzi}	Friction force acting on the cylinder block due to friction between an inidvidual piston and cylinder	[N]
F_{TGi}	Friction force from an individual slipper acting on the cylinder block	[N]
F_{TKi}	Friction force exerted by an individual piston	[N]
$F_{\omega Bi}$	Centrifugal piston force acting on an an individual piston transferred to the cylinder block	[N]
$F_{\omega Ki}$	Centrifugal piston force acting on an individual piston	[N]
K	Bulk Modulus	[Pa]
M_{Bx}, M_{By}	Moment about x and y axes acting on the cylinder block caused by external forces	[Nm]
M_{Bz}	Pump ouput torque	[Nm]
M_{Fx}, M_{Fy}	Moments about the x and y axes caused by fluid force acting on the cylinder block	[Nm]

M_{TBz}	Torque loss due to viscous friction in the cylinder block-valve plate gap	[Nm]
N, M	Number of radial and circumferential grid points in the cylinder block gap surface respectively	[-]
P_f	Power loss due to viscous friction in the cylinder block-valve plate gap	[W]
P_{tot}	Total power loss in the cylinder block-valve plate gap	[W]
P_Q	Power loss due to leakage in the cylinder block-valve plate gap	[W]
Q_{ri}	Net flow into or out of the displacement chamber	[l/min]
Q_{SB}	Leakage from the cylinder block-valve plate gap over one shaft revolution	[l/min]
Q_{SBe1}	Leakage at r = R_{Ba}	[l/min]
Q_{SBe2}	Leakage at r = R_{Bi}	[l/min]
Q_{SBi}	Q_{SB} divided by number of pistons	[l/min]
Q_{SGi}	Leakage from a single slipper-swash plate gap over one shaft revolution	[l/min]
Q_{SKi}	Leakage from a single piston-cylinder gap over one shaft revolution	[l/min]
R	Pitch radius of the cylinder block	[mm]
R_{Ba}	Outer radius of the cylinder block gap surface	[mm]
R_{Bi}	Inner radius of the cylinder block gap surface	[mm]
T_{CASE}	Fluid temperautre in the axial piston pump case	[°C]
T_{HP}	Fluid temperautre at the high pressure port	[°C]
T_{LP}	Fluid temperautre at the low pressure port	[°C]
V_i	Dynamic volume of the displacement chamber	[l]
dC	Circumferential grid spacing for a given radial position	[mm]
f	The waved surface frequency of oscillation	[rev^{-1}]
$\mathbf{f}_B$	Net force acting on the cylinder block	[N]
$h_B(r,\varphi)$	The gap height between the cylinder block and valve plate	[m]
$\boldsymbol{h}_B$	The vector defining the cylinder block position in three points, h_{B1}, h_{B2}, and h_{B3}	[μm]
$h_B(r,\varphi)$	The shifting velocity of the cylinder block	[m/s]
h_{B1}, h_{B2}, h_{B3}	Three points where the gap height between cylinder block and valve plate is calculated	[μm]
h_{max}, h_{min}	Maximum/minimum gap height between the cylinder block and valve plate	[μm]
i, j, k, l	indices	[-]
k_{no}	number of pistons	[-]
n	Pump operating speed	[rpm]
$p(r,\varphi)$	The pressure in the gap	[bar]
p_{HP}	Pressure in the high pressure port	[bar]
p_{LP}	Pressure in the low pressure port	[bar]
p_{case}	Pressure in the displacement unit case	[bar]
p_i	Instantaneous cylinder pressure in the i^{th} cylinder as a function of φ	[bar]
$p_{final}(r,\varphi)$	The final calculated pressure distribution from the Newton iteration	[bar]
r, φ, z	Polar coordinate system for the cylinder block-valve plate gap	[-]
t	Time	[s]
t_0	Start time of the simulation	[s]
t_{end}	User defined time at which to stop a simulation	[s]
t^m	Current time step	[s]
t^{m+1}	Next time step	[s]
$\mathbf{u}_{bDC}$	Deformation of the cylinder block gap surface due to a 100 bar reference pressure applied to the area A_D	[μm]
$\mathbf{u}_{ref}$	Deformation of the cylinder block surface due to a 100 bar reference pressure applied to a small area surrounding a single grid point	[μm]
v_r	Radial component of fluid velocity between cylinder block and valve plate	[m/s]
v_φ	Circumferential component of fluid velocity between cylinder block and valve plate	[m/s]
x	Temporary variable used for calculating the additional gap height for the waved surface	[-]
α_D	orifice coefficient	[-]
β	Swash plate angle (determines the pump displacement)	[%]
$\Delta\mathbf{h}$	Deformation of the cylinder block gap surface	[μm]
Δp	System pressure differential	[bar]
Δt	Time step in the model	[s]
$\Delta\varphi$	Section of the cylinder block surface for calculating deformation	[°]
ε	Tolerance	[-]
μ	Dynamic viscosity of the fluid in the gap	[Pa·s]
ρ	Fluid density	[kg/m^3]
τ	Shear stress of the fluid	[Pa]
τ_r	Shear stress in the radial direction	[Pa]
τ_φ	Shear stress in the circumferential direction	[Pa]
φ	Angular position of the cylinder block	[°]
ω	Angular velocity of the cylinder block	[rad·s^{-1}]

References

Baker, J. 2008. *Power Losses in the Lubricating Gap between Cylinder Block and Valve Plate of Swash Plate Type Axial Piston Machines*, MS thesis, Purdue University.

Baker, J. and **Ivantysynova, M.** 2008. Investigation of Power Losses in the Lubricating Gap between Cylinder Block and Valve Plate of Axial Piston Machines, *Proc. 5th Fluid Power Net International PhD Symposium*, Krakow, Poland, pp. 302-19.

Baker, J. and **Ivantysynova, M.** 2009. Advanced Surface Design for Reducing Power Losses in Axial Piston Machines, *Proc. 11th Scandinavian International Conference on Fluid Power*, Linköping, Sweden, Vol. 10 (2009), No. 2, pp. 15-30.

Bergada, J. M., **Watton, J.** and **Kumar, S.** 2008. Pressure, Flow, Force and Torque Between the Barrel and Port Plate in an Axial Piston Pump, *Journal of Dynamic Systems, Measurement and Control*, Vol. 130, pp. 011011-1-011011-16.

Berthe, D. and **Godet, M.** 1973. A More General Form of Reynolds' Equation-Application to Rough Surfaces. Wear, Vol. 27, pp. 345-57.

Burton, R. A. 1963. Effects of Two-dimensional, Sinusoidal Roughness on the Load Support Characteristics of a Lubricant Film. *Transactions of the ASME, Journal of Basic Engineering*, vol. 85, pp. 258-64.

Dowson, D. and **Ehret, P.** 1999. Past, Present and Future Studies in Elastohydrodynamics. Proceedings of the Institution of Mechanical Engineers, PT.J. *Journal of Engineering Tribology*, Vol. 213, No. J5, pp. 317-33.

Fatu, A., **Hajjam, M.** and **Bonneau, D.** 2005. An EHD Model to Predict the Interdependent Behavior of Two Dynamically Loaded Hybrid Journal Bearings. *Journal of Tribology*, Vol. 127, No. 2, pp. 416-24.

Fredrickson, A. 2008. *A Study of the Piston and Cylinder Interface of an Axial piston Pump Using an Advanced Computer Model*. MS thesis, Purdue University.

Hamrock, B. J., **Schmid, S. R.** and **Jacobson, B. O.** 2004. *Fundamentals of Fluid Film Lubrication*, 2nd Edition. Marcel Dekker, Inc. New York.

Hargreaves, D. J. 1991. Surface Waviness Effects on the Load-carrying Capacity of Rectangular Slider Bearings. Wear, Vol. 145, pp. 137-151.

Harris, M. R., **Edge, K. A.** and **Tilley, D. G.** 1993. Predicting the Behaviour of Slipper Pads in Swashplate-Type Axial Piston Pumps. *ASME Winter Annual Meeting*, New Orleans, Louisiana. 93-WA/FPST-3.

Huang, C. and **Ivantysynova, M.** 2003. A New Approach to Predict the Load Carrying Ability of the Gap Between Valve Plate and Cylinder Block. *Bath Workshop of Power Transmission and Motion Control PTMC 2003*, Bath, UK, pp. 225-39.

Ivantysyn, J. and **Ivantysynova, M.** 2001. *Hydrostatic Pumps and Motors*. Academic Books International, New Delhi.

Ivantysynova, M. 2001. Energy Losses of Modern Displacement Machines - A new approach of Modelling. *Seventh Scandinavian International Conference on Fluid Power*, Linköping, Sweden, pp. 377-95.

Ivantysynova, M. 1999. A New Approach to the Design of Sealing and Bearing Gaps of Displacement Machines. *Fourth JHPS International Symposium on Fluid Power*, Tokyo '99, pp. 45-50.

Ivantysynova, M., **Huang, C.** and **Behr, R.** 2005. Measurements of Elastohydro-Dynamic Pressure Field in the Gap Between Piston and Cylinder. *Bath Workshop on Power Transmission and Motion Control PTMC 2005*, Bath, UK, pp. 451-465.

Jouini, N. and **Ivantysynova, M.** 2008. Valve Plate Surface Temperature Prediction in Axial Piston Machines. *Proc. 5th Fluid Power Net International PhD Symposium*, Krakow, Poland, pp. 95-110.

Lasaar, R. and **Ivantysynova, M.** 2005. An Investigation into Micro- and Macrogeometric Design of Piston/Cylinder Assembly of Swash Plate Machines. *International Journal of Fluid Power*, Vol. 5, no. 1, pp. 23-36.

Lebeck, A. O., **Teale, J. L.,** and **Pierce, R. E.** 1978. Hydrodynamic Lubrication and Wear in Wavy Contacting Face Seals. *Journal of Lubrication Technology*, Vol. 100, pp. 81-91.

Lebeck, A. O. and **Young, L. A.** 1989. Wavy-Tilt-Dam Seal Ring. US Patent 4836561.

Manring, N. D. 2000. Tipping the Cylinder Block of an Axial-Piston Swash-Plate Type Hydrostatic Machine. *Journal of Dynamic Systems, Measurement and Control*, Vol. 122, pp. 216-221.

Patir, N. and **Cheng, H. S.** 1978. An Average Flow Model for Determining Effects of Three Dimensional Roughness on Partial Hydrodynamic Lubrication. *ASME Journal of Lubrication Technology*, Vol. 100, pp. 12-17.

Pelosi, M. and **Ivantysynova, M.** 2009. A Novel Fluid-Structure Interaction Model for Lubricating Gaps of Piston Machines. *Proceedings of the Fifth Fluid Structure Interaction Conference*, Crete. pp. 13-24.

Rasheed, H. 1998. Effect of Surface Waviness of the Hydrodynamic Lubrication of a Plain Cylindrical Sliding Element Bearing. Wear, Vol. 223, pp. 1-6.

Roccatello, A., **Mancò, S.** and **Nervegna, N.** 2007. Modelling a Variable Displacement Axial Piston Pump in a Multibody Simulation Environment.

Journal of Dynamic Systems, Measurement and Control, Vol. 129, pp. 456-468.

Ruddy, A. V., **Dowson, D.** and **Taylor, C. M.** 1982. The Prediction of Film Thickness in a Mechanical Face Seal with Circumferential Waviness on both the Face and the Seat, *Journal Mechanical Engineering Science*, Vol. 24, no. 1, pp. 37-43.

Vaidya, A. and **Sadeghi, F.** 2008. Hydrodynamic Lubrication of Scroll Compressor Thrust Bearing with Grooves and Circular Pockets. *Proc. ASHRAE Annual Meeting*, Salt Lake City, USA.

Yu, T. H. and **Sadgehi, F.** 2001. Groove Effects on Thrust Washer Lubrication. *Journal of Tribology*, Vol. 123, pp. 295-304.

Wieczorek, U. and **Ivantysynova, M.** 2002. Computer Aided Optimization of Bearing and Sealing Gaps in Hydrostatic Machines - The Simulation Tool CASPAR. *International Journal of Fluid Power*, Vol. 3, No. 1, pp. 7-20.

Wohlers, A. and **Murrenhoff, H.** 2007. Tribological Simulation of a Hydrostatic Swash Plate Bearing in an Axial Piston Pump. *Bath Workshop on Power Transmission and Motion Control PTMC 2007*, Bath, UK, pp. 129-141.

Zhao, H., **Choy, F. K.** and **Braun, M. J.** 2005. Dynamic Characteristics and Stability Analysis of a Wavy Thrust Bearing. *Tribology Transactions*, 48:1, pp. 133-139.

Monika Ivantysynova
Born on December 11th 1955 in Polenz (Germany). She received her MSc. Degree in Mechanical Engineering and her PhD. Degree in Fluid Power from the Slovak Technical University of Bratislava, Czechoslovakia. After 7 years in fluid power industry she returned to university. In April 1996 she received a Professorship in fluid power & control at the University of Duisburg (Germany). From 1999 until August 2004 she was Professor of Mechatronic Systems at the Technical University of Hamburg-Harburg. Since August 2004 she is Professor at Purdue University (USA). Her main research areas are energy saving actuator technology and model based optimisation of displacement machines as well as modelling, simulation and testing of fluid power systems. Besides the book "Hydrostatic Pumps and Motors" published in German and English, she has published more than 80 papers in technical journals and at international conferences.

Jonathan Baker
Born in North Carolina, Jonathan received his bachelor's degree in Physics from Davidson College and Master's degree in mechanical engineering from Purdue University under the guidance of Professor Monika Ivantysynova at the Maha Fluid Power Research Center. His research interests are related to pump efficiency and lubricating gap design.